

# On the mechanism of metal combustion in nitrogen

*I.A.Filimonov<sup>1</sup> and N.I. Kidin<sup>2</sup>*

<sup>1</sup> *Institute of Structural Macrokinetics and Materials Science RAS, Chernogolovka,  
142432 Russia, e-mail: fil\_limonov@hotmail.com*

<sup>2</sup> *Institute for Problems in Mechanics RAS, Moscow, 117526 Russia,  
e-mail: kidin@ipmnet.ru*

## **Abstract**

A model explaining and predicting generation of a temporal electric potential during nitridation of a single metal pellet has been developed. The model takes into account the kinetics of defects formation and assumes that the rate of the chemical reaction can be described by the shrinking-core process.

The model simulations have shown that the time scale of the generated electric potential depends on both the initial nitride shell thickness and heat removal from the particle surface. At thin initial shell and low rate of heat removal the maximum of the surface electric potential is attained before the temperature and surface nitrogen concentration have reached their maximums but after the maximum of nitridation has appeared. At thick initial shell and/or high rates of heat removal from the particle surface the potential maximum is observed much later: after the maximum temperature has been achieved.

In contrast to oxidation the nitrogen adsorption rate constants (the activation energy and pre-exponent) have a negligible effect on the surface potential form and amplitude. At the ignition limit the rate of nitridation is proportional to the power of  $-1/2$  for the ambient nitrogen pressure in the proposed scheme of defects formation. Metal vacancies and electron holes are the main charged defects in nitrides during nitrogen combustion. The nitride formation is limited by transfer of metal vacancies in nitride.

## **Introduction**

In recent years a growing need has appeared for high power electronic devices capable of operation at high temperatures and caustic environments. This led to renewed efforts directed towards III-V nitrides research.

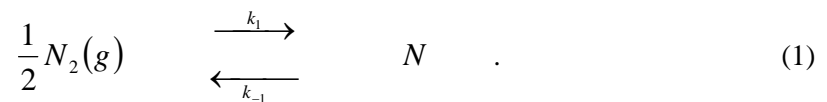
The kinetics of the high-temperature Ti, Zr, Nb and Ta nitridation at the early combustion stages was studied in details [1-3]. It was revealed [3] that the rate of the TaN film growth was proportional to the power of  $-1/2$  for nitrogen pressure. Therefore the authors concluded that neutral nitrogen vacancies were mainly responsible for mass transfer during high-temperature tantalum nitridation. The same mechanism of nitrogen diffusion is implied for other metals [4,5]. Nevertheless, there are data contradicting the conclusion [3]. The data on the defects and transport properties of nitrides [6] show that nitrogen diffusion and nitride formation are limited by transfer of metal vacancies in nitride.

These vacancies are usually charged negatively. Moreover, like in oxygen [7,8] the self-generation of a transient electric voltage was observed during the Ti combustion in nitrogen [9,10]. One cannot explain this voltage taking into account only the neutral vacancies.

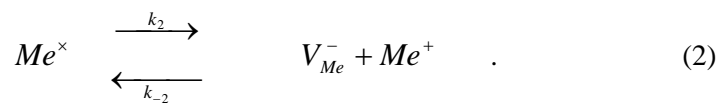
We present a paper suggesting a mechanism of defects formation in nitrides through metal vacancies. Using this mechanism in model [11,12] we have succeeded in explanation of the electrical field generation during the high-temperature nitridation of metal particles [9,10] and implicitly confirm data [6]. The discrepancy with the conclusion [3] is discussed.

### Governing equations

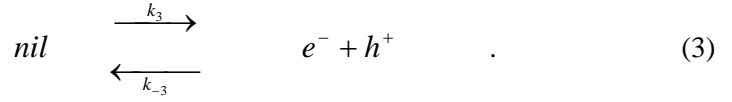
We consider the high-temperature nitridation of a spherical metal particle of radius  $R_0$ . Since the Pilling-Bedworth (nitride to metal density) ratio is very close to unity [13,14] the particle radius is supposed to be a constant during the reaction. Assume also that absorbed nitrogen diffuses through the nitride layer in the form of neutral interstitial atoms and reacts with metal at the metal-nitride interface (Fig. 1). Dependent on the particle temperature and ambient nitrogen pressure the electrons and/or electron holes may provide the nitride conductivity. For example, increasing the nitrogen flux leads to transition from strongly conductive to a semi-insulating state in GaN [15] (Fig. 2). Strong n-type conductivity with high concentrations of free electrons is replaced by phonon-assisted hopping among the localized defects in this case (Table 1). We assume that the rate of metal nitridation is very fast relative to the metal cation (vacancy) diffusion rate so that the nitride shell growth can be described by the shell progressive model [16]. The ambient gaseous nitrogen is adsorbed on the pellet surface via the reversible reaction



Interstitial metal cations and metal vacancies are formed in the nitride lattice by the reactions



Simultaneously, electron-hole pairs are generated via thermal ionization



Different diffusion rates of charge carriers ( $Me^+$ ,  $e^-$  and  $V_{Me}^-$ ,  $h^+$ ) produce an electric charge in the nitride shell. The metal cations and electrons are consumed or produced by a reaction at the metal core (radius  $R_{Me}$ ):



In the case of low defect concentrations (lower than the equilibrium ones), this reaction generates metal cations, electrons and interstitial nitrogen atoms. Vice versa, the metal nitride, vacancies and electron holes are formed.

We assume that the temperature within the particle is uniform but different from the ambient gas, and that neither melting nor phase transformations occur. The reaction network (1)-(4) postulates the nitridation kinetics with defects and accounts for the information [3,6] about their charge and mobility.

The reaction rates satisfy the following relations:

$$W_1 = -\frac{1}{2} \frac{d[N_{2,g}]}{dt} = k_1 [N_{2,g}]^{1/2} - k_{-1} [N] \quad (5)$$

$$W_2 = \frac{d[Me^\times]}{dt} = -\frac{d[Me^+]}{dt} = k_{-2} [Me^+] \cdot [V_{Me}^-] - k_2 [Me^\times] \quad (6)$$

$$W_3 = \frac{d[e^-]}{dt} = k_3 - k_{-3} [e^-] \cdot [h^+] \quad (7)$$

$$W_4 = \frac{d[MeN_\nu]}{dt} = k_4 [Me^+] [e^-] [N]^\nu - k_{-4} [MeN_\nu] \quad (8)$$

The lattice metal concentration,  $[Me^\times]$ , may be assumed to be a constant [17]. In addition, we assume that the concentrations of electrons ( $e^-$ ) and electron holes ( $h^+$ ) attain a quasi-steady state, i.e.,

$$W_i = 0, \quad i = 2, 3. \quad (9)$$

The nitrogen concentration near the pellet surface,  $[N_{2,g}]$ , satisfies the relation

$$W_1 = k_c \left( [N_{2,g}]^\infty - [N_{2,g}] \right), \quad (10)$$

where  $k_c$  is the mass transfer coefficient and  $[N_{2,g}]^\infty$  is the ambient concentration of gaseous nitrogen.

In accordance with equations (5)-(10) the electrochemical equilibrium concentrations of reactions (1)-

(4) at the reference temperature  $T^*$  chosen as the temperature rise due to nitridation

( $T^* = (-\Delta H)/(\rho_{cond} C)$ ) are

$$[N]^* = \frac{k_1(T^*)}{k_{-1}(T^*)} \left( [N_{2,g}]^\infty \right)^{1/2}, \quad (11)$$

$$[V_{Me}^-]^* = [h^+]^* = \left( \frac{k_{-2}(T^*)}{k_2(T^*)} \frac{k_{-3}(T^*)}{k_3(T^*)} \frac{k_{-4}(T^*)}{k_4(T^*)} [MeN_\nu]^* \right)^{-1/2} \left( \frac{k_1(T^*)}{k_{-1}(T^*)} \right)^{\nu/2} \left( [N_{2,g}]^\infty \right)^{\nu/4}, \quad (12)$$

$$[e^-]^* = \left( \frac{k_{-2}(T^*)}{k_2(T^*)} \frac{k_{-3}(T^*)}{k_3(T^*)} \frac{k_{-4}(T^*)}{k_4(T^*)} [MeN_\nu]^* \right)^{1/2} \left( \frac{k_1(T^*)}{k_{-1}(T^*)} \right)^{-\nu/2} \left( [N_{2,g}]^\infty \right)^{-\nu/4}. \quad (13)$$

$$[Me^+]^* = \left( \frac{k_2(T^*)}{k_{-2}(T^*)} \frac{k_3(T^*)}{k_{-3}(T^*)} \frac{k_4(T^*)}{k_{-4}(T^*)} [MeN_\nu]^* \right)^{1/2} \left( \frac{k_1(T^*)}{k_{-1}(T^*)} \right)^{-\nu/2} \left( [N_{2,g}]^\infty \right)^{-\nu/4}, \quad (14)$$

Using relations (11)-(14) one can calculate the critical value of  $[MeN_\nu]^*$  providing close

concentrations of the charge carriers ( $k_2(T^*)/k_{-2}(T^*) \approx k_3(T^*)/k_{-3}(T^*)$ )

$$[MeN_\nu]_c^* = \left( \frac{k_2(T^*)}{k_{-2}(T^*)} \frac{k_4(T^*)}{k_{-4}(T^*)} \right) \left( \frac{k_1(T^*)}{k_{-1}(T^*)} \right)^\nu \left( [N_{2,g}]^\infty \right)^{\nu/2}. \quad (15)$$

At high nitrogen pressures this value is extremely large, therefore, the metal vacancies ( $V_{Me}^-$ ) and

electron holes ( $h^+$ ) are the main contributors to electrical charge transport in nitrides, i.e.

$$[V_{Me}^-]^* \gg [Me^+]^* \text{ and } [h^+]^* \gg [e^-]^* \text{ at } [MeN_\nu]^* \ll [MeN_\nu]_c^*. \quad (16)$$

Alternatively, the interstitial metal cations ( $Me^+$ ) and electrons ( $e^-$ ) are mainly generated and are responsible for voltage formation at low nitrogen pressures:

$$[Me^+]^* \gg [V_{Me}^-]^* \text{ and } [e^-]^* \gg [h^+]^* \text{ at } [MeN_v]^* \gg [MeN_v]_c^*. \quad (17)$$

It is well known that sufficiently high gas pressures are necessary to ignite small metal particles in nitrogen. Correspondingly, we consider here operation conditions (16). At intermediate nitrogen concentrations when  $[MeN_v]^* \approx [MeN_v]_c^*$ , one has to account for all four charge carriers (metal cations, vacancies, electron holes and electrons).

Solving equations. (5), (10)-(13) we get

$$y = \frac{A(\theta)^2}{4} \left( \left[ 1 + \frac{4}{A(\theta)^2} + \frac{4 \cdot \chi \cdot z}{A(\theta)} \right]^{1/2} - 1 \right)^2. \quad (18)$$

where

$$y = [N_{2,g}] / [N_{2,g}]^\infty, \quad z = [N] / [N]^*, \quad \theta = T / T^*, \quad (19)$$

$$\gamma_1 = \frac{E_1}{RT^*}, \quad \gamma_{-1} = \frac{E_{-1}}{RT^*}, \quad k_i(\theta) = k_i^0 \cdot \exp(-\gamma_i / \theta), \quad i = +1, -1,$$

$$\chi = \frac{k_1(1) k_{-1}(\theta)}{k_1(\theta) k_{-1}(1)} = \exp\left\{(\gamma_{-1} - \gamma_1) \cdot \left(1 - \frac{1}{\theta}\right)\right\},$$

$$A_0 = \frac{k_1(1)}{k_c \left([N_{2,g}]^\infty\right)^{1/2}}, \quad A = A_0 \exp\left\{\gamma_1 \left(1 - \frac{1}{\theta}\right)\right\}.$$

It predicts that no nitrogen adsorption occurs ( $y \rightarrow 1$ ) either at low-temperatures ( $A \rightarrow 0$ ) or when the surface concentration of interstitial nitrogen atoms tends to the equilibrium values ( $z \rightarrow z_e, z_e = \chi^{-1}$ ). According to (19) the difference in the activation energies of the adsorption and desorption rate constants determines the behavior of the surface nitrogen concentration at the later stages of combustion, when this concentration tends to equilibrium and the temperature drops. For

$\gamma_{-1} < \gamma_1$  the concentration drops with decreasing the temperature ( $\theta < 1$ ) and vice versa for  $\gamma_{-1} > \gamma_1$ .

The steady-state non-dimensional boundary conditions on the particle surface are

$$\left(\nabla_{\xi} n\right)_{\xi=1} = 0, \quad \left(\nabla_{\xi} p\right)_{\xi=1} = 0 \quad \text{at } \xi = 1, \quad (20)$$

$$\beta_z \cdot \left(\nabla_{\xi} z\right)_{\xi=1} = 1 - y \quad \text{at } \xi = 1, \quad (21)$$

where

$$\xi = r / R_0, \quad n = \left[V_{Me}^{-}\right] / \left[V_{Me}^{-}\right]^*, \quad p = \left[h^{+}\right] / \left[h^{+}\right]^*, \quad (22)$$

$$\beta_z = \left(\frac{D_z}{2R_0}\right) \cdot \left(\frac{k_1(T^*)}{k_{-1}(T^*)}\right) / \left(k_c [N_{2,g}]^{\infty 1/2}\right),$$

The electric potential distribution satisfies the Poisson equation:

$$\Lambda^2 \cdot \Delta_{\xi\xi} \phi - n + p = 0, \quad (23)$$

$$\text{where} \quad \phi = e\varphi / kT^*, \quad \Lambda = \left\langle \frac{kT_0}{4\pi \cdot e^2} \frac{1}{R_0^2} \frac{1}{\left[h^{+}\right]^* N_A} \right\rangle^{1/2}. \quad (24)$$

The distributions of charge carriers and a neutral defect within the nitride shell satisfy the transient diffusion equations,

$$\frac{\partial n}{\partial \tau} = \bar{D}_- \cdot \left\{ \nabla_{\xi}^2 n - \nabla_{\xi} \left( \frac{n}{\theta} \nabla_{\xi} \phi \right) \right\}, \quad (25)$$

$$\frac{\partial p}{\partial \tau} = \nabla_{\xi}^2 p + \nabla_{\xi} \left( \frac{p}{\theta} \nabla_{\xi} \phi \right), \quad (26)$$

$$\frac{\partial z}{\partial \tau} = \bar{D}_z \cdot \nabla_{\xi}^2 z, \quad (27)$$

$$\text{where} \quad \tau = t \cdot D_+ / R_0^2, \quad \bar{D}_- = D_- / D_+, \quad \bar{D}_z = D_z / D_+. \quad (28)$$

The Poisson-Nernst-Planck equations [18-20] are the steady-state version of (23)-(26). In contrast to the oxidation model [12] diffusion of neutral interstitial nitrogen atoms is additionally considered. Charge conservation at the particle surface and the metal-nitride interface is a boundary condition, i.e.,

$$\left(\frac{\partial \phi}{\partial \xi}\right) = p - n, \quad \text{at} \quad \xi = 1. \quad (29)$$

$$\left(\frac{\partial \phi}{\partial \xi}\right) = 0, \quad \text{at} \quad \xi = \xi_{Me}. \quad (30)$$

At thin initial nitride shells and high initial temperatures reaction (4) is strongly shifted to the nitride formation and can be treated as an irreversible one under operating conditions (16). The atoms of nitrogen are consumed by a very fast reaction at the shrinking metal core (metal-nitride interface), i.e.,

$$z = 0, \quad \text{at} \quad \xi = \xi_{Me} > 0, \quad (31)$$

$$\left(\nabla_{\xi} z\right)_{\xi=\xi_{Me}} = -\beta_{+} \left( \nabla_{\xi} p + \frac{p}{\theta} \nabla_{\xi} \phi \right)_{\xi=\xi_{Me}}, \quad \text{at} \quad \xi = \xi_{Me} > 0, \quad (32)$$

$$\left(\nabla_{\xi} z\right)_{\xi=\xi_{Me}} = -\bar{D}_{-} \beta_{+} \left( \nabla_{\xi} n - \frac{n}{\theta} \nabla_{\xi} \phi \right)_{\xi=\xi_{Me}}, \quad \text{at} \quad \xi = \xi_{Me} > 0, \quad (33)$$

$$\text{where} \quad \beta_{+} = [h^{+}]^{*} / (\bar{D}_{z} [N]^{*}). \quad (34)$$

When all the metal has been consumed, these boundary conditions are replaced by

$$\frac{\partial z}{\partial \xi} = \frac{\partial n}{\partial \xi} = \frac{\partial p}{\partial \xi} = 0, \quad \xi \equiv 0. \quad (35)$$

The molar consumption rate of the metal is  $1/\nu$  of that of the nitrogen atoms. Thus,

$$\frac{d\xi_{Me}}{d\tau} = -I \cdot \bar{D}_{z} \cdot \left(\nabla_{\xi} z\right)_{\xi=\xi_{Me}}, \quad I = \frac{M_w}{\nu \rho} [N]^{*}. \quad (36)$$

The non-dimensional form of the thermal balance is:

$$\frac{d\theta}{d\tau} = -3\xi_{Me}^2 \frac{d\xi_{Me}}{d\tau} + H_0 \int_0^1 (\xi \nabla_{\xi} \phi)^2 d\xi - H_1 (\theta - \theta_{00}) - H_2 (\theta^4 - \theta_{00}^4), \quad (37)$$

where

$$H_0 = 3 \left( \frac{k}{C\rho_{cond} \cdot e} \right)^2 \frac{\sigma_{el} (-\Delta H)}{D_{+}}, \quad H_1 = \frac{\alpha}{C\rho_{cond}} \frac{3R_0}{D_{+}}, \quad H_2 = \frac{\varepsilon\sigma}{(C\rho_{cond})^4} \cdot (-\Delta H)^3 \frac{3R_0}{D_{+}}. \quad (38)$$

The terms on the RHS of (37) account for the chemical reaction, Joule dissipation, thermal convection and radiation, respectively. Like for oxidation [12] the temperature rise by Joule dissipation is ignored i.e., we assume  $H_0 = 0$ . The model consists of equations (23),(25)-(27) subject to boundary conditions (20),(21),(31)-(35) for the defect concentrations and (29), (30) for the electric potential. Ordinary differential equations (36) and (37) describe the changes in  $\xi_{Me}$  and  $\theta$ . The initial conditions are:

$$z = n = p = \phi \equiv 0, \quad \theta = \theta_0 \quad \text{at} \quad \tau = 0, \quad \forall \xi. \quad (39)$$

Elliptic equation. (23) was treated as a parabolic one using the relaxation method [21] with a very small time constant ( $\bar{\varepsilon} = 10^{-4}$ ). It was integrated simultaneously with others by the method of finite differences. The equations were transformed into a tridiagonal set of linear algebraic equations and were integrated using the Crank and Nicholson method [22] with a uniform finite difference grid (up to 500 nodes). These were solved by the Thomas algorithm [23,24].

## Numerical results

We used numerical simulations to study the evolution of the metal vacancies and electron holes, temporal temperature and electric potential during the high-temperature nitridation of a single metal particle. Assuming that the particle is initially heated to a temperature at which the intrinsic rate of the chemical reaction greatly exceeds that of the interstitial nitrogen diffusion, we may adequately apply the shrinking core model to description of the metal nitridation rate. We assume also that neither melting nor a phase transformation occurs during the reaction and that a thin nitride layer is formed before the combustion has started. Our goal is to reveal the evolution of an electric voltage during the metal nitridation and to understand the relation between the particle temperature rise and the temporal electric potential formation.

In this paper we consider mainly the effects of nitridation rate and heat removal. Therefore we present here our simulations only for  $\bar{D}_-^0 = 1.81$ ,  $E_{\bar{D}_-} = 0.8$ ,  $\bar{D}_z \equiv 0.1$ ,  $\beta_+ \equiv 0.25$ ,  $\beta_z \equiv 1.5$ ,  $\gamma_1 = 8$ ,  $\gamma_{-1} = 5$ ,  $\Lambda \equiv 0.01$ ,  $\theta_0 = 0.5$ ,  $\theta_{00} = 0.15$ ,  $H_1 = 0.01$  and  $I \equiv 10.1$ . Fig. 3a illustrates the typical transient temperature ( $\theta$ ), conversion degree ( $\eta$ ) and the rate of nitridation ( $\delta\eta/\delta\tau$ ), actual

concentration of the surface adsorbed nitrogen ( $z[1]$ ) and its deviation from the equilibrium values ( $z_e[1] - z[1]$ ) as well as the surface electric potential ( $\phi[1]$ ) during the combustion at low rate of heat losses from the particle surface. Such conditions correspond to combustion of a single metal particle with a thin initial nitride shell in gaseous nitrogen. In this case the characteristic time scale of the surface electric potential is much less than those of temperature, conversion degree and concentration of adsorbed nitrogen. The maximum of the surface electric potential ( $\phi_m[1] \cong -1.07$ ) is attained before the temperature and adsorbed nitrogen have reached their maximums but after that of the nitridation rate. The potential vanishes with time. These results are completely similar to those for oxygen combustion [12] and can be explained by strongly non-equilibrium concentrations of metal vacancies and electron holes the most intensively produced during the initial nitridation stage ( $\tau|_{\phi_m} \cong 0.05$ ) when the nitridation rate maximum has been achieved. Next we will see that at a thin initial nitride shell and a low rate of heat losses the vacancy and hole concentrations attain the equilibrium values by the time at which the maximum temperature ( $\theta_m \cong 1.35$ ) has been achieved ( $\tau|_{\theta_m} \cong 2.0$ ). Vice versa is the adsorbed nitrogen (Fig. 3a). The nitrogen concentration close to equilibrium initially deviates sufficiently from it at the maximum temperature ( $z_e[1]|_{\theta_m} - z[1]|_{\theta_m} \cong 1.9$ ) and only later tends to be equilibrium.

The same behavior for adsorbed nitrogen is revealed at large coefficients of heat transfer (Fig. 3b). Nevertheless, under these conditions the maximum temperature is sufficiently lower ( $\theta_m \cong 0.81$ ) and the nitrogen deviation from equilibrium decreases sharply ( $z_e[1]|_{\theta_m} - z[1]|_{\theta_m} \cong 0.39$ ). The time at which the maximum temperature is achieved decreases also ( $\tau|_{\theta_m} \cong 0.51$ ) while the rate of nitridation as well as the surface potential at the initial combustion stage ( $\tau < 0.15$ ) is about equal to that at low rates of heat removal. Due to the fact that the characteristic time of heat removal for such a particle greatly exceeds that of the nitridation reaction, the effect of large heat transfer coefficients is observed after the initial stage only ( $\tau \geq 0.15$ ). In addition to the temperature and the adsorbed nitrogen concentrations, the surface potential and nitridation rate change drastically during this later stage. The

potential drops to the value ( $\phi_m[1] \cong -4.54$ ) exceeding those calculated both at the initial stage and with low rates of heat removal from the particle surface. The second surface potential maximum is attained much later than the maximum temperature has achieved and its characteristic time scale correlates to the combustion time ( $\tau|_{\phi_m} \cong 3.5$ ).

To reveal the reason of the surface electric potential behavior at large coefficients of heat transfer we consider the metal-nitride interface (Fig. 4). At the small coefficients and low rates of heat removal from the particle surface (Fig. 4a) the vacancy and hole concentrations on the interface ( $n[\xi_{Me}]$  and  $p[\xi_{Me}]$ ) distinguish noticeably each other at the initial combustion stage only ( $\tau < 0.15$ ) and are almost identical during the later combustion. This means that quasi-neutral equilibrium profiles of the charge carriers are established by the end of the initial combustion stage ( $\tau \cong 0.15$ ). Correspondingly, no electric charge and potential are generated inside the particle by that time. The interface temporal electric potential ( $\phi[\xi_{Me}]$ ) as well as the  $n[\xi_{Me}] - p[\xi_{Me}]$  difference has only one maximum and vanishes with increasing  $\tau$ . All the interstitial nitrogen arriving to the interface is consumed by the reaction. Therefore condition  $z[\xi_{Me}] = 0$  holds till the metal has been completely exhausted, i.e. till the end of the combustion time ( $\tau_c \cong 2.44$ ). An increase in concentration of the interface interstitial nitrogen after that moment ( $z[\xi_{Me}] \cong 0.4$  at  $\tau = 4$ ) is caused by transition to chemical equilibrium and the particle cooling.

In the same way the interface nitrogen behaves at large coefficients of heat transfer (Fig. 4b). The only difference is that the scale of  $z[\xi_{Me}]$  (and temperature) changes is much smaller:  $z[\xi_{Me}] < \cong 0.61$ . In contrast to low rates of heat losses the interface vacancy and hole concentrations are strongly non-equilibrium and there is a strong difference between them during all the combustion time. Therefore the metal-nitride interface generates an electric charge and potential all the time. Moreover, the interface carrying charge converges to the particle center hence it causes formation of the second peak in the  $n[\xi_{Me}] - p[\xi_{Me}]$  difference ( $\langle n[\xi_{Me}] - p[\xi_{Me}] \rangle_m \cong 0.01$ ) and the second electric potential maximum ( $\phi_m[\xi_{Me}] \cong -4.54$ ). This maximum appears to be much stronger than the first one and has

the characteristic time close to  $\tau_c$ . The potential in the vicinity of the first maximum ( $\phi_m[\xi_{Me}] \cong -1.05$ ) remains identical to that at low rates of heat removal till the end of the initial combustion stage ( $\tau < 0.15$ ).

All the results presented in Figs. 3,4 correspond to the particle with the same thin initial nitride shell ( $\xi_{Me}^0 = 0.98$ ). Therefore both the nitridation rate and electric potential during the initial combustion stage do not change under the increase in heat removal. To prove more evidently that the potential generation at this stage is primary related to the defect diffusion rates and the rate of nitridation, in Fig. 5 we consider the effect of the initial nitride shell thickness. The nitridation starts (Fig. 5a) with a delay and its maximum rate is sufficiently lower  $[\delta\eta/\delta\tau]_m \cong 0.08$  and shifted to longer times ( $\tau \cong 0.64$ ) at the increased initial thickness ( $\xi_{Me}^0 = 0.48$ ). The surface electric potential is generated with the same delay ( $\tau \cong 0.2$ ) and the decreased first potential maximum ( $\phi_m[1] \cong -0.87$ ). The adsorbed nitrogen concentration approaching the equilibrium values during the delay deviates from them until the maximum temperature has been reached ( $\tau \cong 2.34$ ). The deviation maximum is small ( $z_e[1]_{\theta_m} - z[1]_{\theta_m} \cong 0.018$ ) relative to that at the thin initial nitride shell.

Processes on the metal-nitride interface (Fig. 5b) start earlier and the corresponding delay for them is shorter ( $\tau \cong 0.14$ ) than for those on the particle surface. Qualitatively, the transient defect concentrations and the interface electric potential are very similar to those at the thin initial nitride shell and large coefficient of heat transfer (Fig. 4b). The only difference is the delay in rises of defect concentrations and electric potential as well as a very small discrepancy between the concentrations of metal vacancies and electron holes ( $\langle n[\xi_{Me}] - p[\xi_{Me}] \rangle_m \cong 0.003$ ). Accordingly, both the first ( $\phi_m[\xi_{Me}] \cong -0.93$ ) and second ( $\phi_m[\xi_{Me}] \cong -3$ ) maximums of electric potential are smaller than those at the thin initial shell and high rates of heat removal.

In contrast to oxidation [12] the activation energies of nitrogen adsorption as well as the adsorption rate constants have a negligible effect on the surface potential form and amplitude. The reason is that the metal-nitride interface but not the particle surface serves as the main source of

defects during nitridation. Therefore changes in the surface kinetics have no such effect like on formation of oxides with a mixed electronic-ionic conductivity [12].

Fig. 6 describes the dimensionless dependence of the initial rate of nitridation on the adsorption rate pre-exponent for two thicknesses of the initial nitride shell. One can see that this dependence may be treated as a linear one at small values of the pre-exponent when the nitridation proceeds at the limit of ignition. In accordance with relation (19) this means that at the limit of ignition the rate of the nitride film growth is proportional to the power of  $-1/2$  for the ambient nitrogen pressure. Thus, we have numerically obtained the result similar to that observed in experiments [3] while no neutral nitrogen vacancies have been considered. Therefore the only proportionality observed [3] is not an experimental fact sufficient for identification of the mechanism of nitrogen diffusion in nitrides.

### **Concluding remarks**

Thus, the characteristic time of electric potential generated during the high-temperature nitridation of a single metal particle strongly depends on the conditions of heat removal from the particle surface and the initial nitride shell thickness. At thin initial shell and low rates of heat removal this time is much shorter than those at which the temperature and the surface nitrogen concentration have reached their maximums. At thick initial shell and/or high rates of heat removal from the particle surface electric potential is still generated after the maximum temperature has been achieved. While the first conditions correspond most likely to combustion of a single metal particle in gaseous nitrogen, the second ones may be attributed to nitridation of powder samples. Unfortunately, no nitridation experiments in powders letting the comparison of transient electric potentials for these powders and single particles are known. Nevertheless, the results obtained in experiments on oxidation of metals [7,8] are qualitatively in a good agreement with our conclusion.

Concentrations of the metal vacancies and electron holes produced by the reaction of nitride formation at the metal-nitride interface determine the rate of nitridation. The larger the values of these concentrations, the higher is the nitridation rate. An increase in the coefficients of heat transfer shifts the concentration maximums to longer times and retards nitridation. Thicker initial nitride shells cause

lower defect concentrations and a delay in the concentration rises. This also increases the combustion time.

The higher the particle temperature, the shorter is the time for the vacancy and hole concentrations to attain the equilibrium values. At higher temperatures metal vacancies and electron holes form quasi-neutral pairs faster and electric potential disappears in a shorter time. At sufficiently low temperatures the hole-vacancy interaction is so weak that strong non-equilibrium concentrations of the vacancies and holes exist till the end of nitridation and the electric potential is generated all the combustion time.

### Acknowledgment

We thank the Russian Fund of Basic Research (RFBR) for financial support of this work in the frames of RFBR grant N 05-03-33180-a.

### Notation

#### Symbols

- $A$  - dimensionless nitrogen adsorption rate, defined by Eq. (19)
- $A_0$  - dimensionless adsorption pre-exponent, defined by Eq. (19)
- $C$  - specific heat capacity,  $J / (kg \cdot K)$
- $\bar{D}_z$  - dimensionless diffusion coefficient of neutral carriers, defined by Eq. (28)
- $\bar{D}_-$  - dimensionless diffusion coefficient of negative carriers, defined by Eqs. (28)
- $\bar{D}_z^0, \bar{D}_-^0$  - dimensionless pre-exponents of  $\bar{D}_z$  and  $\bar{D}_-$ , respectively
- $D_i$  - diffusion coefficients,  $m^2/s$
- $E_i$  - activation energy,  $J / mole$
- $E_{\bar{D}_k}$  - dimensionless activation energy of  $\bar{D}_k$
- $e$  - electron/ electron charge, C
- $h$  - electron hole
- $H_0$  - dimensionless Joule heating coefficient, defined by Eq. (38)
- $H_1$  - dimensionless convective heat transfer coefficient, defined by Eq. (38)
- $H_2$  - dimensionless radiative heat transfer coefficient, defined by Eq. (38)
- $\Delta H$  - heat of reaction,  $J / m^3$
- $I$  - dimensionless maximum surface nitrogen flux, defined by Eq. (36)
- $k$  - Boltzmann constant,  $J / K$
- $k_i$  - reaction rate constants in Eqs. (1)-(4)
- $k_c$  - mass-transfer coefficient,  $m/s$
- $Me^+$  - interstitial metal cation
- $M_w$  - molecular weight,  $kg / mole$
- $n$  - dimensionless metal vacancies concentration, defined by Eq. (22)
- $N$  - nitrogen
- $N_A$  - Avogadro number

$p$  - dimensionless concentration of electron holes, defined by Eq. (22)  
 $r$  - radial coordinate,  $m$   
 $R$  - universal gas constant,  $J/(K \cdot mole)$   
 $R_0$  - external radius of spherical pellet,  $m$   
 $R_{Me}$  - shrinking metal core radius,  $m$   
 $T$  - temperature,  $K$   
 $t$  - time,  $s$   
 $W_i$  - surface reaction rate,  $mole/(m^2 s)$   
 $V_{Me}^-$  - metal vacancy  
 $y$  - dimensionless nitrogen concentration

### Greek Symbols

$\alpha$  - heat transfer coefficient,  $J/(m^2 \cdot s \cdot K)$   
 $\beta_z$  - dimensionless nitrogen atoms molar surface flux, defined by Eq. (22)  
 $\beta_+$  - dimensionless molar flux of electron holes at metal-nitride interface, defined by Eq. (34)  
 $\gamma_1$  - dimensionless adsorption activation energy, defined by Eq. (19)  
 $\gamma_{-1}$  - dimensionless desorption activation energy, defined by Eq. (19)  
 $\varepsilon$  - emissivity  
 $\eta$  - conversion  
 $\phi$  - dimensionless electric potential, defined by Eq. (24)  
 $\varphi$  - electric potential,  $V$   
 $\Lambda$  - dimensionless Debye screening length, defined by Eq. (24)  
 $\nu$  - stoichiometric index  
 $\theta$  - dimensionless temperature, defined by Eq. (19)  
 $\rho_{cond}$  - condensed phase density,  $kg/m^3$   
 $\sigma_{el}$  - electric conductivity,  $1/(\Omega \cdot m)$   
 $\sigma$  - Stefan-Boltzmann constant,  $J/(m^2 \cdot s \cdot K^4)$   
 $\tau$  - dimensionless time, defined by Eqs. (28)  
 $\xi$  - dimensionless radial coordinate, defined by Eq. (22)  
 $\chi$  - dimensionless ratio of adsorption-desorption rate constants, defined by Eq. (19)

### Subscripts and Superscripts

$c$  - metal consumption time  
 $e$  - equilibrium values  
 $g$  - gaseous  
 $m$  - maximum values  
 $Me$  - at the metal-nitride interface  
 $0$  - initial value  
 $00$  - ambient temperature  
 $1$  - surface  
 $\xi_{Me}$  - interface  
 $\times$  - lattice  
 $*$  - equilibrium concentrations  
 $-/+$  - electric charge of defects  
 $\infty$  - ambient concentration

## References

- [1] Kharatyan SL, Grigoriev YuM, Merzhanov AG (1975) Titanium ignition in nitrogen. In *Physics of Combustion and Explosion*, vol. 11, no 1, pp. 26-33.
- [2] Merzhanov AG, Grigoriev YuM, Kharatyan SL et al. (1975) Investigation of the kinetics of heat release at high-temperature nitridation of zirconium filaments. In *Physics of Combustion and Explosion*, vol. 11, no 4, pp. 563-568
- [3] Vadchenko SG, Grigoriev YuM, Merzhanov AG (1980) The effect of pressure on the kinetics of high-temperature tantalum nitridation. In *Metals*, no 1, pp. 194-196.
- [4] Thiers L, Leitenberger BJ, et al. (2000) Influence of preheating rate on kinetics of high-temperature gas-solid reactions. In *AIChE Journal*, vol. 46, no 12, pp. 2518-2524.
- [5] Pelekh AE, Mukasyan AS, Varma A (1999) Kinetics of rapid high-temperature reactions: titanium-nitrogen system. In *Ind. Eng. Chem. Res.*, vol. 38, pp. 793-799.
- [6] Matzke Hj (1989) Point defects and transport properties in carbides and nitrides. In Johannesen O and Andersen AG (eds) *Studies in Inorganic Chemistry 9. Selected Topics in High Temperature Chemistry. Defect Chemistry of Solids*. Elsevier, Amsterdam - Oxford - New York - Tokyo, pp. 353-385.
- [7] Nersesyanyan MD, Ritchie JT, Filimonov IA, Richardson JT, Luss D (2002) Electric fields produced by high-temperature metal oxidation. In *Journal of the Electrochemical Society*, vol. 149, no 1, pp. J11-J17.
- [8] Martirosyan KS, Filimonov IA, Nersesyanyan MD, Luss D (2003) Electric field formation during combustion of single metal particles. In *Journal of the Electrochemical Society*, vol. 150, no 5, pp. J9-J16.
- [9] Setoodeh M, Martirosyan KS, Luss D (2003) Formation of electric field during the combustion of titanium in nitrogen. In XVIII Annual OChEGS Symposium, Houston, USA, Book of Abstracts, p.14.
- [10] Vadchenko SG, Filimonov IA et al. (2005) Electric voltage generation during inflammation of titanium in nitrogen. In 4<sup>th</sup> Mediterranean Combustion Symposium, Instituto Superior Tecnico, Lisbon, Portugal, Book of Abstracts, paper P1-04.
- [11] Filimonov IA, Luss D (2004) Electrical field formation during the oxidation of a metal particle. In *AIChE (American Institute of Chemical Engineers) Journal*, vol. 50, no 9, pp. 2287-2296.
- [12] Filimonov IA, Luss D (2005) High-temperature oxidation of a metal particle: nonisothermal model. In *AIChE (American Institute of Chemical Engineers) Journal*, vol. 51, no 5, pp. 1521-1531.
- [13] Rode H, Orlicki D, Hlavacek V (1995) Noncatalytic gas-solid reactions and mechanical stress generation. In *AIChE (American Institute of Chemical Engineers) Journal*, vol. 41, no. 5, pp. 1235-1250.
- [14] Rode H, Hlavacek V (1994) An experimental study of titanium powder reactivity in gaseous environments. In *Combust. Sci. and Tech.*, vol. 99, pp. 143-160.
- [15] Look DC, Reynolds DC, Kim W, Aktas O, Botchkarev A, Salvador A, Morkoc H (1996) Deep-center hopping conduction in GaN. In *J. Appl. Phys.*, vol. 80, no. 5, pp. 2960-2963.
- [16] Levenspiel O (1972) *Chemical Reaction Engineering*. John Wiley, NY.
- [17] Gellings PJ, Bouwmeester HJM (eds) (1997) *The CRC Handbook of Solid State Electrochemistry*, CRC Press, Boca Raton - New York - London - Tokyo.
- [18] Jerome JW (1985) Consistency of Semiconductor Modeling: an Existence/Stability Analysis for the Stationary Van Roosbroek System. In *SIAM J. Appl. Math.*, vol. 45, no. 4, pp. 565-591.
- [19] Barcion V, Chen D-P, Eisenberg RS, Jerome JW (1997) Qualitative properties of steady-state Poisson-Nernst-Planck systems: perturbation and simulation study. In *SIAM J. Appl. Math.*, vol. 57, no. 3, pp. 631-648.
- [20] Park J-H, Jerome JW (1997) Qualitative properties of steady-state Poisson-Nernst-Planck systems: mathematical study. In *SIAM J. Appl. Math.*, vol. 57, no. 3, pp. 609-630.
- [21] Press WH, Flannery BP, Teukolsky SA, Vetterling WT (1993) *Numerical Recipes in C: The Art of Scientific Computing*. Cambridge University Press, 2nd edition.

- [22] Crank J, Nicholson P (1947) In Proc. Cambridge Philos. Soc., vol. 43, pp. 50-67; [Re-published in: John Crank 80<sup>th</sup> birthday special issue (1997) Adv. Comput. Math., vol. 6, pp. 207-226].
- [23] Thomas LH (1949) Elliptic problems in linear difference equations over a network. In Watson Sci. Comput. Lab. Rept., Columbia University, New York.
- [24] Ames WF (1977) Numerical Methods for Partial Differential Equations (Second Edition). Academic Press, New York.

Sample	$T_{\text{sub}}$	N flux ( $\text{cm}^{-2} \text{s}^{-1}$ )	$d(\mu\text{m})$	$\rho(\Omega \text{ cm})$	$\mu_H$ ( $\text{cm}^2/\text{V s}$ )	$n_H$ ( $\text{cm}^{-3}$ )
5169	750 °C	$5.5 \times 10^{15}$	3.8	$4.3 \times 10^{-2}$	$1.3 \times 10^2$	$1.1 \times 10^{18}$
5176	750 °C	$1.6 \times 10^{16}$	5.3	$1.4 \times 10^1$	3.5	$1.3 \times 10^{17}$
5175	750 °C	$3.4 \times 10^{16}$	5.3	$3.1 \times 10^3$ <sup>a</sup>	...	...
5069	800 °C	unknown	6.0	$1.9 \times 10^6$ <sup>a</sup>	...	...

<sup>a</sup>Hopping conduction.

Table 1 Properties of GaN layers grown at different fluxes of nitrogen including 296 K values of  $\rho, \mu$  and  $n$  [15]

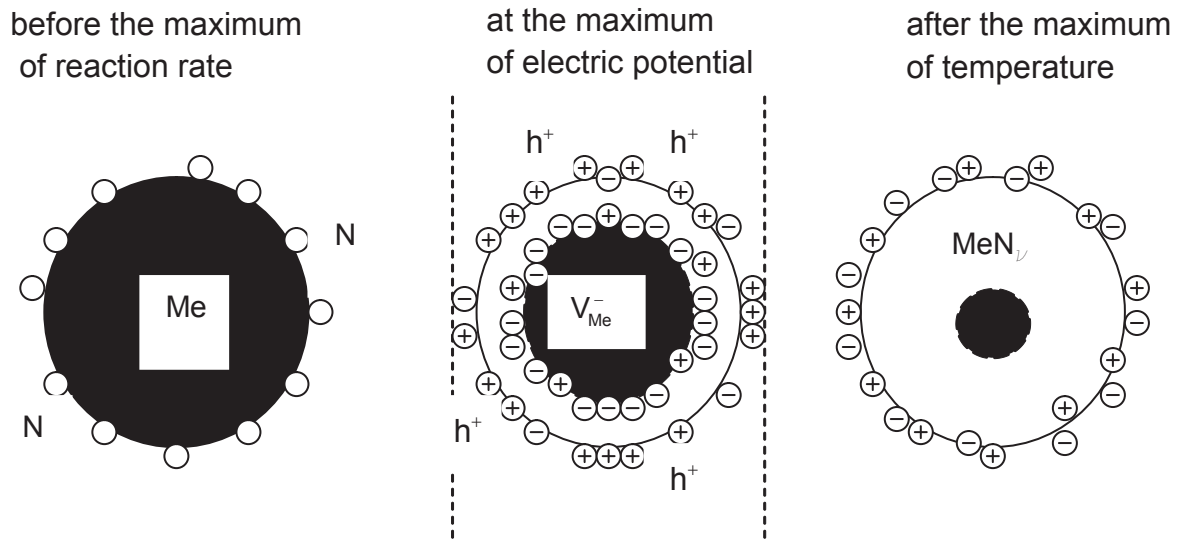


Fig.1 Double charge layer formation during combustion of metal particles in nitrogen

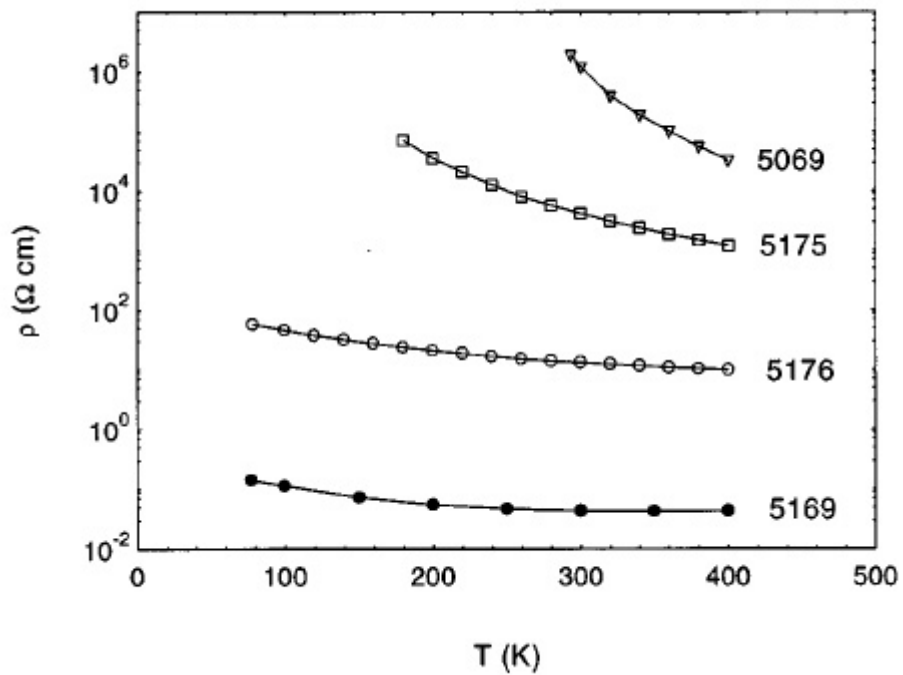


Fig.2 Resistivity for various GaN layers [15]. The upper curves represent samples grown with higher nitrogen fluxes (see Table 1).

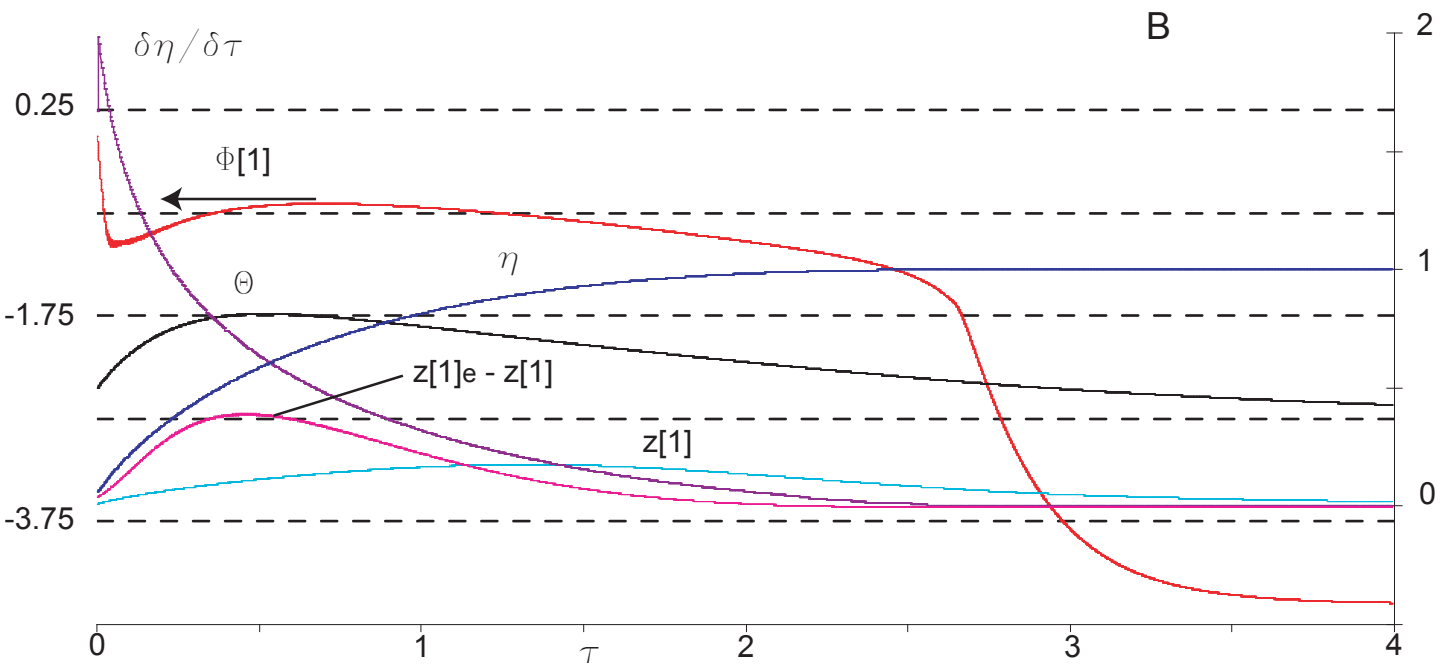
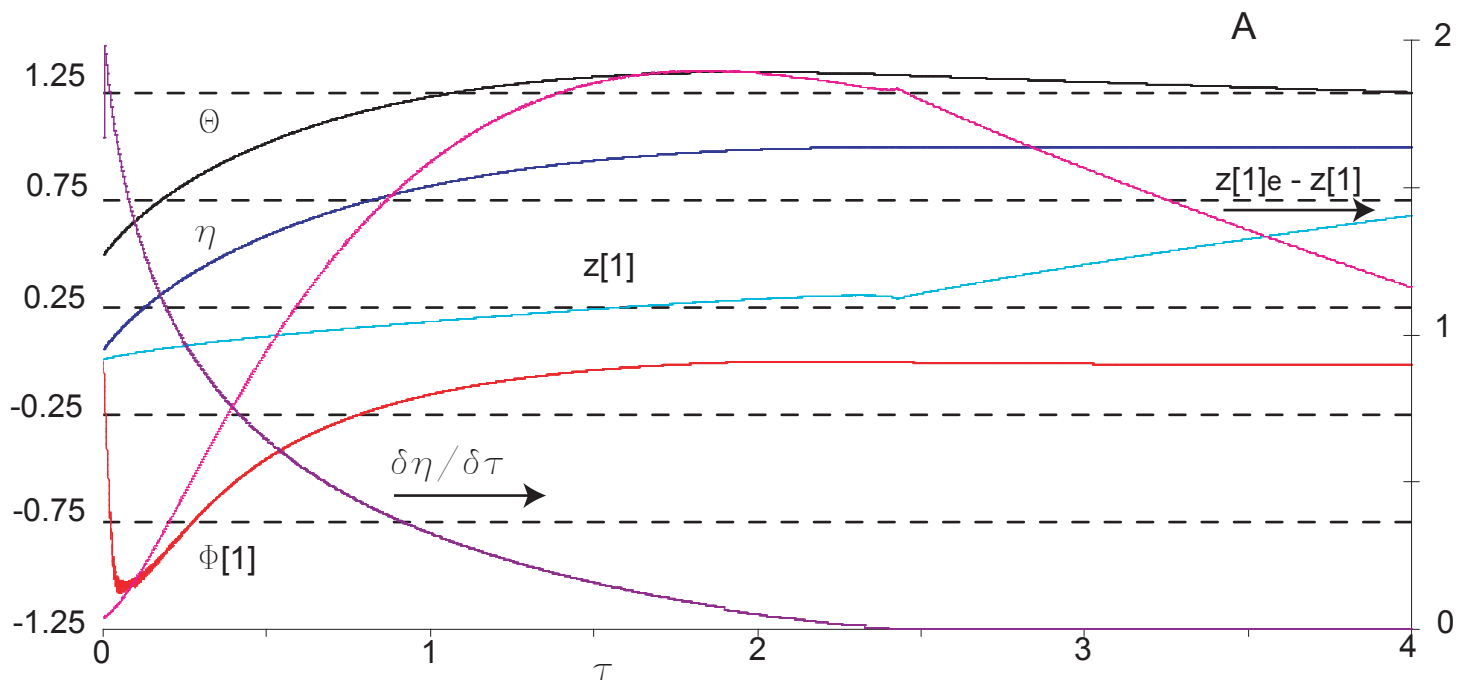


Fig. 3 Typical transient temperature ( $\theta$ ), conversion degree ( $\eta$ ), nitridation rate ( $\delta\eta/\delta\tau$ ), actual ( $z[1]$ ) and equilibrium ( $z[1]e$ ) concentrations of the surface adsorbed nitrogen, surface electric potential ( $\Phi[1]$ ) during combustion of a metal particle in nitrogen at low (a) and high (b) coefficient of heat transfer.  $\xi_{Me}^0 = 0.98$ ,  $A_0 = 10^5$ , a)  $H_2 = 0.01$ , b)  $H_2 = 1.08$

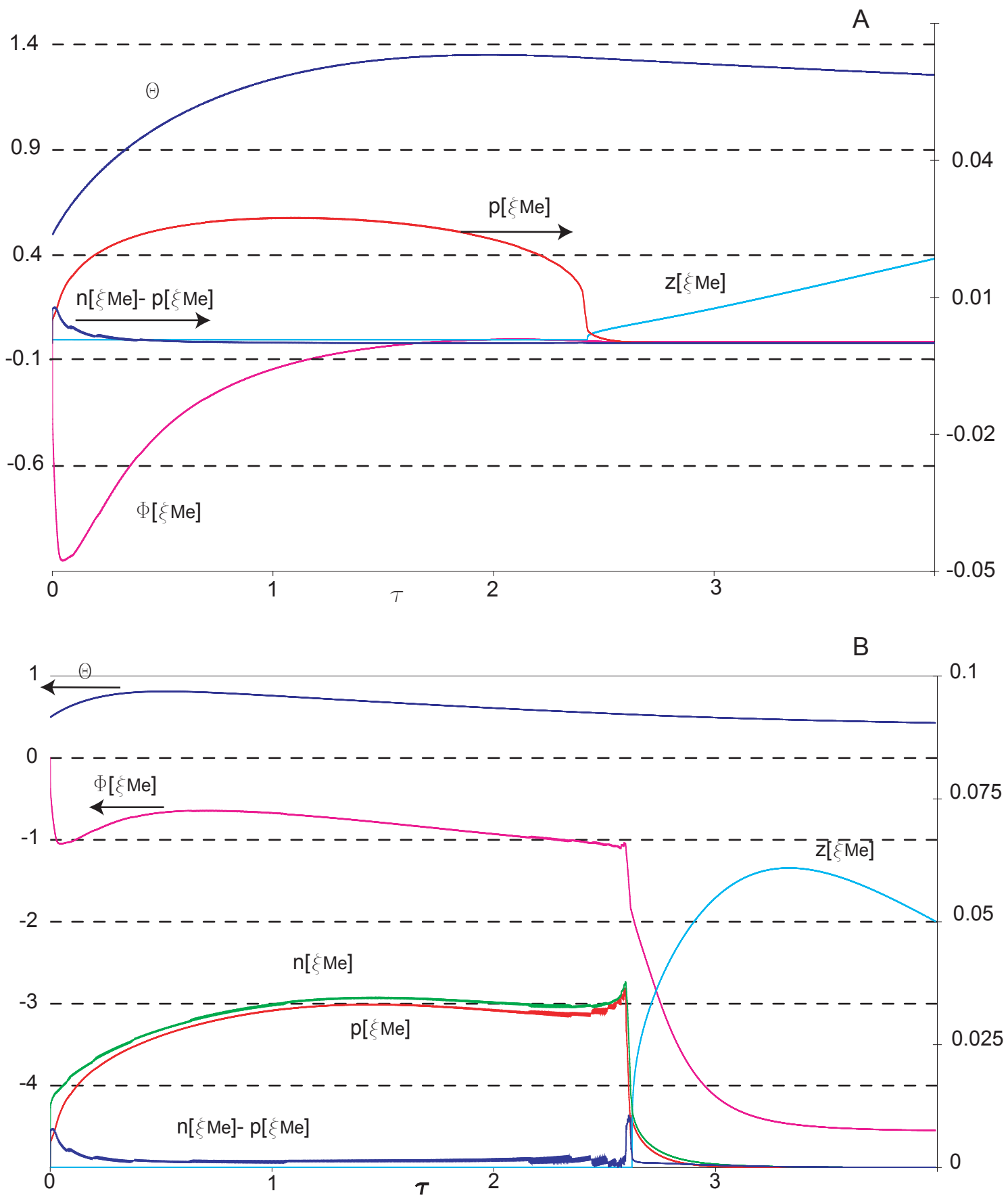


Fig. 4 Typical transient temperature ( $\Theta$ ), concentrations of the interstitial nitrogen ( $z[\xi\text{Me}]$ ), electron holes ( $p[\xi\text{Me}]$ ) and metal vacancies ( $n[\xi\text{Me}]$ ) as well as electric potential ( $\Phi[\xi\text{Me}]$ ) at the metal-nitride interface during combustion of a metal particle in nitrogen at low (a) and high (b) coefficient of heat transfer.  
 $\xi_{\text{Me}}^0=0.98$ ,  $A_0=10^5$ , a)  $H_2=0.01$ , b)  $H_2=1.08$

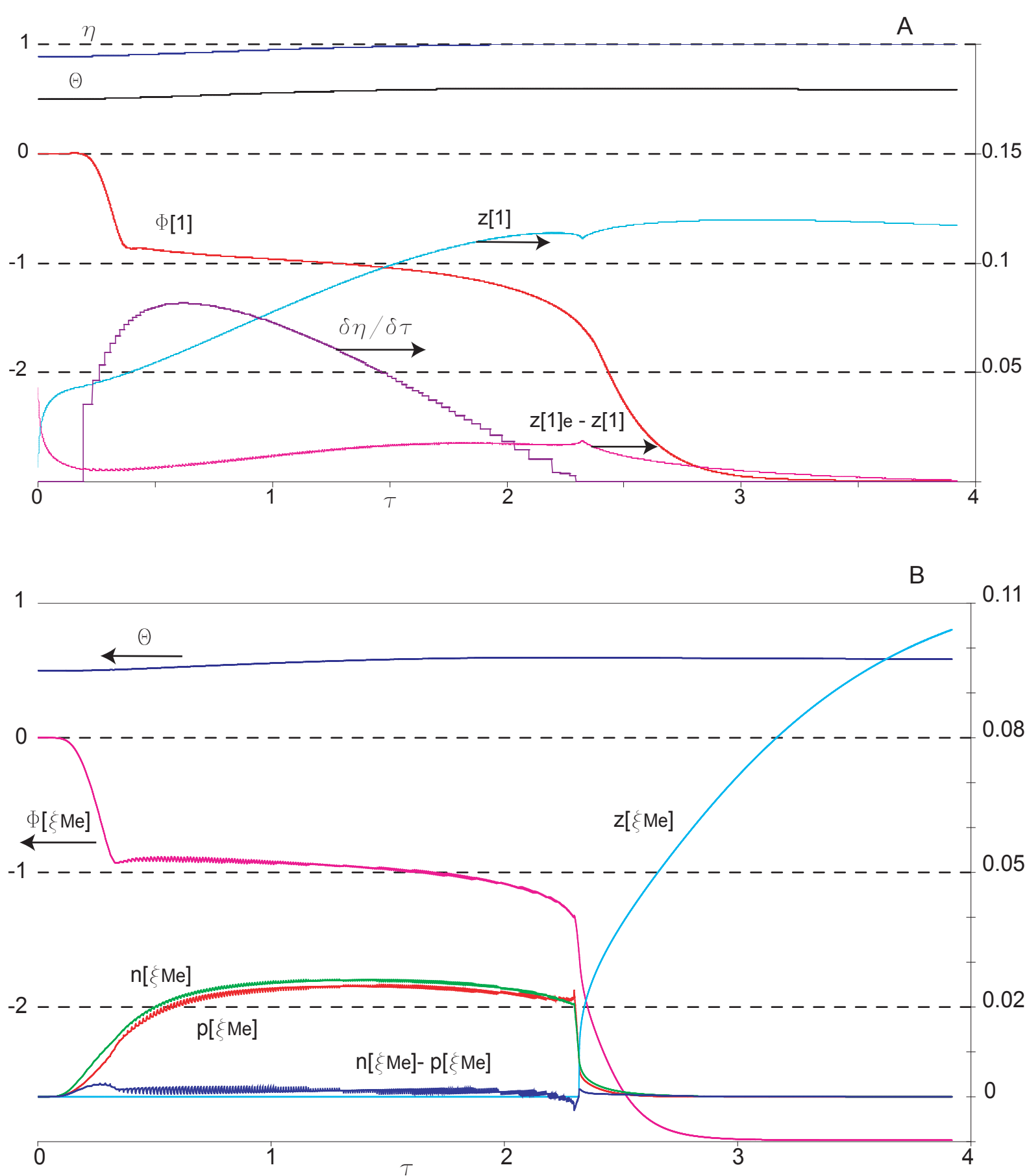


Fig. 5 Nitridation of a metal particle with the thick initial nitride shell ( $\xi_{Me}^0=0.48$ ,  $A_0=10^5$ ,  $H_2=0.01$ ). Variation of the surface (a) and metal-nitride interface (b) values. Typical transient temperature ( $\Theta$ ), degree of conversion ( $\eta$ ), nitridation rate ( $\delta\eta/\delta\tau$ ), concentrations of the interstitial nitrogen ( $z$ ), electron holes ( $p$ ) and metal vacancies ( $n$ ) as well as electric potential ( $\Phi$ ).

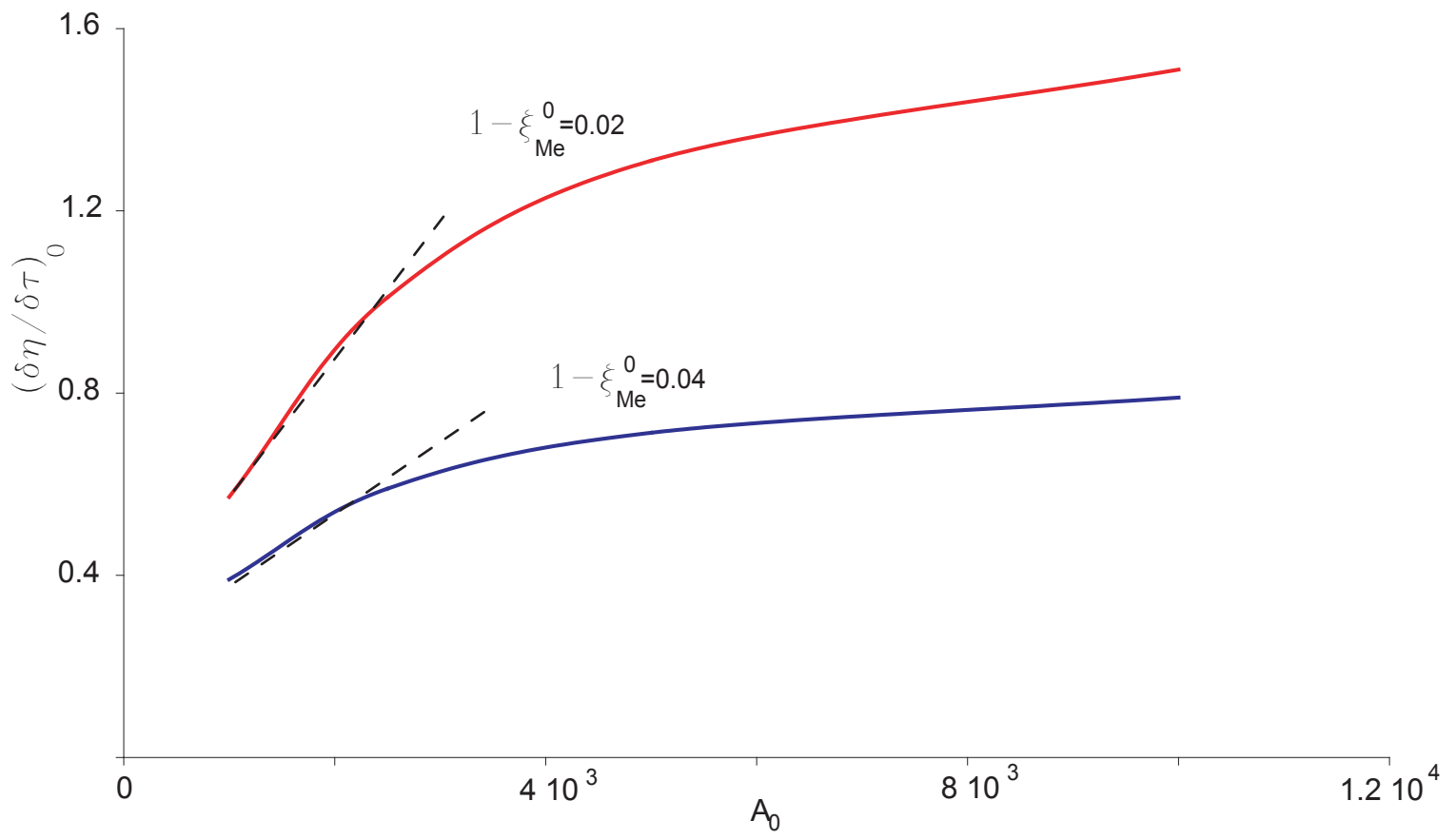


Fig. 6 Initial nitridation rate as the function of adsorption pre-exponent  $H_2 = 0.01$ .